the major signature of the 15 April flare on Earth was the elimination of reliable ionospheric data.

More continuous data sets exist for the 26 April flare, and they show the expected enhancements of the E layer electron densities by the flare. At Sondrestrom, the site most appropriate for comparisons with MGS at Mars, the electron density increased by ~45%. Because the E layer is caused by both EUV and soft x-rays and the EUV changed only slightly, the Sondrestrom results must be due to the more-than-double effective ionizing fluxes, in agreement with Eq. 1 applied at Mars. We conclude that these two flares produced near-simultaneous enhancements in the ionospheres of Earth and Mars and that the greater relative increase at lower altitudes in Mars' $N_e(h)$ is consistent with the typical flare spectrum of greater relative flux increases at shorter wavelengths. The N_e increase at Mars is also consistent with the enhancement at its corresponding site on Earth.

The detection of solar flare effects in the martian ionosphere has important consequences. Previous observations and modeling of the responses of planetary ionospheres to changes in solar flux have generally compared solar maximum and minimum conditions. Varying solar fluxes also modify the neutral atmosphere, and thus ionospheric changes result from two highly coupled processes. Although simulations can separate the dependence on each of these parameters, validation from observations over a solar cycle cannot. The observations presented here decouple changes in photon flux due to a flare from far slower changes in the neutral atmosphere, thereby providing a way to constrain photochemistry on two planets simultaneously. This is particularly important for x-ray photons that carry energy far above that needed to ionize an atom or molecule. In such cases, the electron liberated by ionization has so much extra energy that it ionizes other atoms and molecules via collisions. This secondary ionization by photoelectrons is an amplification effect that needs validation throughout the solar system. For Venus, Earth, and Mars, where ionospheric layers have identical end product ions (O_2^+), solar flares offer tests for both primary and secondary ionization coupled to an identical chemical loss mechanism. Calculations using the same solar flare input thus provide constraints not possible at a single planet.

References and Notes
1. R. Prange et al., Nature **432**, 78 (2004).
2. A. Bhardwaj et al., Geophys. Res. Lett. **32**, 10.1029/2004GL021497 (2005).
3. A. Bhardwaj et al., Astrophys. J. **624**, L121 (2005).
4. H. Rishbeth, O. K. Garriott, Introduction to Ionospheric Physics (Academic Press, New York, 1969).
5. R. Schunk, A. Nagy, Ionospheres (Cambridge Univ. Press, Cambridge, 2000).
6. R. F. Donnelly, Sol. Phys. **20**, 188 (1971).
7. N. R. Thomson, C. J. Rodger, R. L. Dowden, Geophys. Res. Lett. **31**, 10.1029/2003GL019345 (2004).
8. M. Mendillo, S. Smith, J. Wroten, H. Rishbeth, D. Hinson, J. Geophys. Res. **108**, 10.1029/2003JA009961 (2003).
9. C. R. Martinis, J. K. Wilson, M. Mendillo, J. Geophys. Res. **108**, 10.1029/2003JA009973 (2003).
10. D. P. Hinson, R. A. Simpson, J. D. Twicken, G. L. Tyler, F. M. Flasar, J. Geophys. Res. **104**, 26997 (1999).
11. P. L. Bornmann et al., Proc. SPIE **2812**, 309 (1996).
12. J. Fox, J. Geophys. Res. **109**, 10.1029/2004JA010380 (2004).
13. P. C. Chamberlin, T. N. Woods, F. G. Eparvier, abstract SA34A.08, 2005 American Geophysical Union (AGU) Fall Meeting, San Francisco, CA, 5 to 9 December 2005.
14. D. L. Judge, H. S. Ogawa, D. R. McMullin, P. Gangopadhyay, J. M. Pap, Adv. Space Res. **29**, 1963 (2002).
15. B. W. Reinisch, in Modern Ionospheric Science, H. Kohl, R. Ruster, K. Schlegel, Eds. (European Geophysical Society, Katlenburg-Lindau, Germany, 1996), pp. 440–458.
16. At Boston University, this work was supported by NASA's Mars Data Analysis Program (M.M., H.R., and P.W.) and from NSF's Coupling, Energetics, and Dynamics of Atmospheric Regions program (P.W.). At Stanford University, support is from the NASA MGS program. At the University of Massachusetts, Lowell, support for the ionosonde observations comes from U.S. Air Force grant no. f19628-C-0092. We are grateful for data analysis provided by J. Wroten (Boston University) and G. Khmyrov (University of Massachusetts, Lowell) and acknowledge use of GOES data from http://sec.noaa.gov/Data/goes.html and SOHO data from www.usc.edu/dept/space_science/semdata.htm.

Anthropogenic and Natural Influences in the Evolution of Lower Stratospheric Cooling

V. Ramaswamy,[1] M. D. Schwarzkopf,[1] W. J. Randel,[2] B. D. Santer,[3] B. J. Soden,[4] G. L. Stenchikov[5]

Observations reveal that the substantial cooling of the global lower stratosphere over 1979–2003 occurred in two pronounced steplike transitions. These arose in the aftermath of two major volcanic eruptions, with each cooling transition being followed by a period of relatively steady temperatures. Climate model simulations indicate that the space-time structure of the observed cooling is largely attributable to the combined effect of changes in both anthropogenic factors (ozone depletion and increases in well-mixed greenhouse gases) and natural factors (solar irradiance variation and volcanic aerosols). The anthropogenic factors drove the overall cooling during the period, and the natural ones modulated the evolution of the cooling.

The global lower stratosphere—the region of the atmosphere from ~12 to 22 km above the surface—has cooled substantially over the past two decades (1–5). The difference in temperature between 2000 and 1979 has been ascribed mainly to ozone depletion and increases in well-mixed greenhouse gases (4, 6–10). Observations indicate that the decrease in temperature was steplike rather than a steady decline (1, 3). Although the overall trend in temperature has been modeled previously (5, 9, 10), the steplike structure and the evolution of the cooling pattern in the observed global temperature time series has not been explained in terms of specific physical causes, whether these be external forcing and/or internal variability of the climate system. Thus, attribution of the unusual cooling features observed during the 1980s and 1990s has yet to be addressed, along with potential implications for the future.

We used a coupled atmosphere-ocean model (11–13) to demonstrate that the complex space-time pattern of the lower stratospheric temperature anomalies is a consequence of the combined temporal changes in natural forcings [solar irradiance (14) and volcanic aerosols (15)] and anthropogenic forcings [well-mixed greenhouse gases (16), stratospheric (17) and tropospheric ozone (18), tropospheric aerosols (18), and land use (13)].

We performed five separate experiments to investigate the contributions of different forcing mechanisms to changes in lower stratospheric temperature: (i) natural plus anthropogenic (AllForc), (ii) natural (Nat), (iii) well-mixed greenhouse gases (Wmgg), (iv) well-mixed greenhouse gases plus stratospheric and tropospheric ozone (WmggO3), and (v) anthropogenic (Anth; that is, WmggO3 plus tropospheric aerosols and land-use change). For each case, an ensemble of simulations was performed. Individual ensemble members started from different points of a long control simulation with a fixed preindustrial (1860) atmospheric composition and were then integrated from 1861 through 2003. There were five ensemble members for (i);

[1]National Oceanic and Atmospheric Administration/Geophysical Fluid Dynamics Laboratory, Princeton, NJ 08542, USA. [2]National Center for Atmospheric Research, Boulder, CO 80303, USA. [3]Program for Climate Model Diagnosis and Intercomparison, Lawrence Livermore National Laboratory, Livermore, CA 94550, USA. [4]Rosentiel School for Marine and Atmospheric Science, University of Miami, Miami, FL 33149, USA. [5]Department of Environmental Sciences, Rutgers University, New Brunswick, NJ 08901, USA.
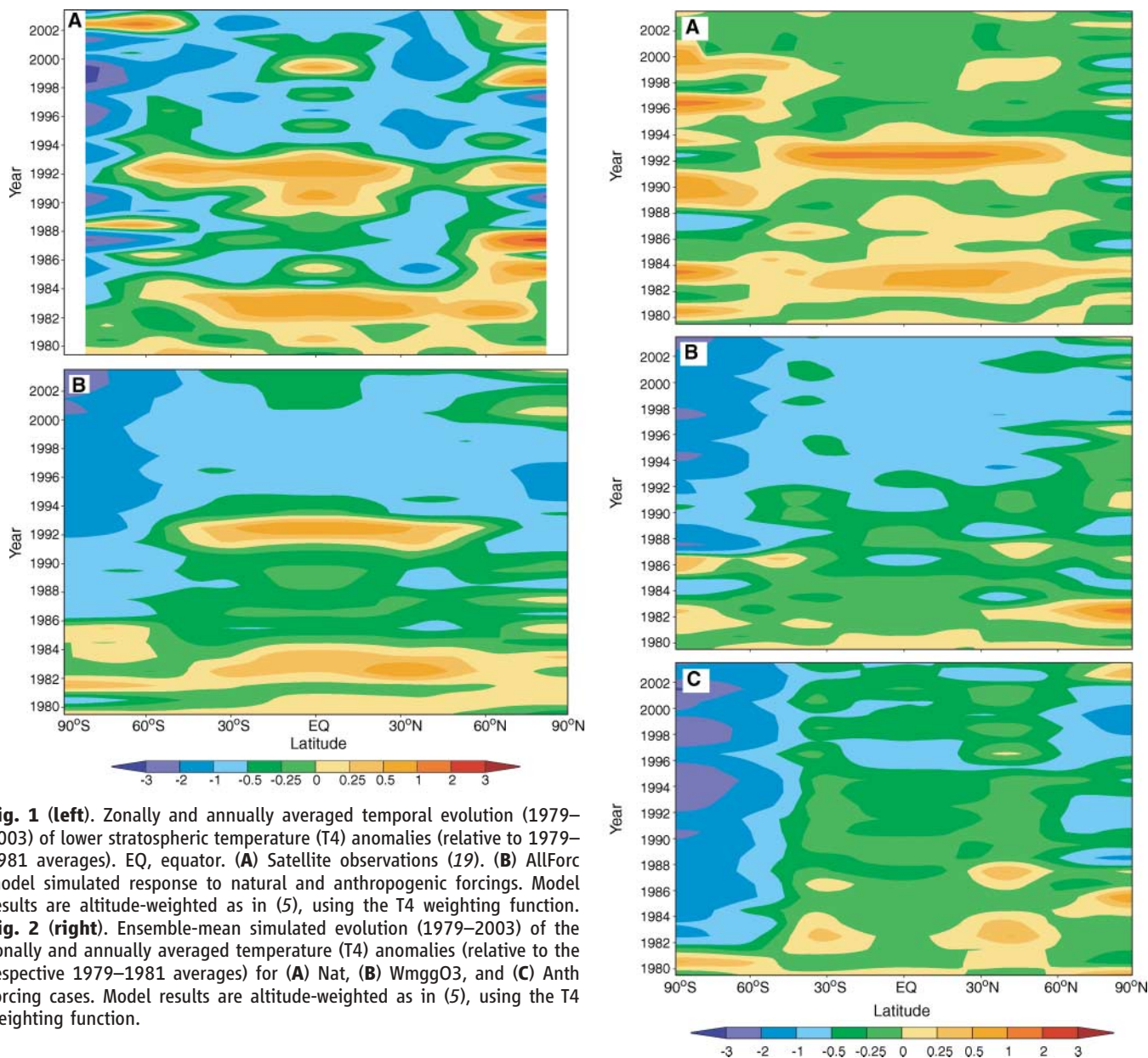
Fig. 1 (left). Zonally and annually averaged temporal evolution (1979–2003) of lower stratospheric temperature (T4) anomalies (relative to 1979–1981 averages). EQ, equator. (**A**) Satellite observations (*19*). (**B**) AllForc model simulated response to natural and anthropogenic forcings. Model results are altitude-weighted as in (*5*), using the T4 weighting function. **Fig. 2 (right)**. Ensemble-mean simulated evolution (1979–2003) of the zonally and annually averaged temperature (T4) anomalies (relative to the respective 1979–1981 averages) for (**A**) Nat, (**B**) WmggO3, and (**C**) Anth forcing cases. Model results are altitude-weighted as in (*5*), using the T4 weighting function.

(ii) to (v) comprised three members each, starting from the same initial conditions as three of the AllForc integrations. The observed lower stratospheric temperatures (1979–2003) were from measurements (referred to as T4) made by channel 4 of the Microwave Sounding Unit on the National Oceanic and Atmospheric Administration's satellites (*19*). Synthetic T4 values were computed from the simulated temperature profiles as described in (*5*). The observed and simulated T4 results are expressed as annual mean temperature anomalies, relative to their respective 1979–1981 averages.

The observed time evolution of the zonally and annually averaged T4 temperature anomalies (Fig. 1A) illustrates the transient warming in ~1982–1984 and ~1991–1993 after the El Chichon (1982) and Pinatubo (1991) volcanic eruptions. This warming resulted from the radiative effects of the stratospheric sulfate aerosols formed after the eruptions (*4*, *9*, *10*). After the decay of the volcanic aerosols (~2 years after eruption), the warming ceased, and the lower stratosphere in the 50°N-50°S domain cooled substantially relative to the pre-eruption period. After the steplike transition in ~1985, the observed T4 values were relatively stable until the Pinatubo eruption. The decay of the Pinatubo-related warming was followed by a second steplike cooling in T4 (~1994), and the anomaly remained approximately steady thereafter. The signature of the quasi-biennial oscillation (QBO) in temperature, a natural mode of climate variation (*20*), was clearly manifested at the equator. There was large dynamical variability at high latitudes, especially in the Northern Hemisphere (*4*, *21*).

The AllForc simulation (Fig. 1B) captures the primary features of the observed T4 anomalies, including the El Chichon and Pinatubo warming anomalies; the two steplike cooling transitions; and the ensuing prolonged, quasi-steady periods (~1985–1990 and ~1994–2000). The simulated evolution is spatially more homogeneous and exhibits less cooling than do observations made in the 1980s; the widespread extent and increased cooling in the 1990s is broadly consistent with observations. As in the observations, the model shows both cooling and substantial dynamical variability poleward of 50° (*4*, *6–8*). The model lacks a QBO and hence does not replicate the observed periodicity of T4 near the equator.

The simulated influences due to the key forcings are illustrated in Fig. 2. As expected, Nat shows a large stratospheric warming after El Chichon and Pinatubo, but no overall trend (Fig. 2A). In contrast, WmggO3 and Anth (Fig. 2,

1139

Fig. 3. (**A**) Model-simulated ensemble-mean (AllForc, red curve) and Microwave Sounding Unit (MSU, black curve) satellite observations (*19*) of the globally and annually averaged temperature (T4) anomalies over 1979–2003 (relative to their respective 1979–1981 averages). The gray shading denotes the range of the five-member ensemble simulations and is a measure of the simulated internally generated variability of the climate system. (**B**) Model-simulated ensemble mean of the globally and annually averaged temperature (T4) anomalies (relative to the respective 1979–1981 averages) for the AllForc, Nat, Wmgg, WmggO3, and Anth radiative forcing cases, respectively.
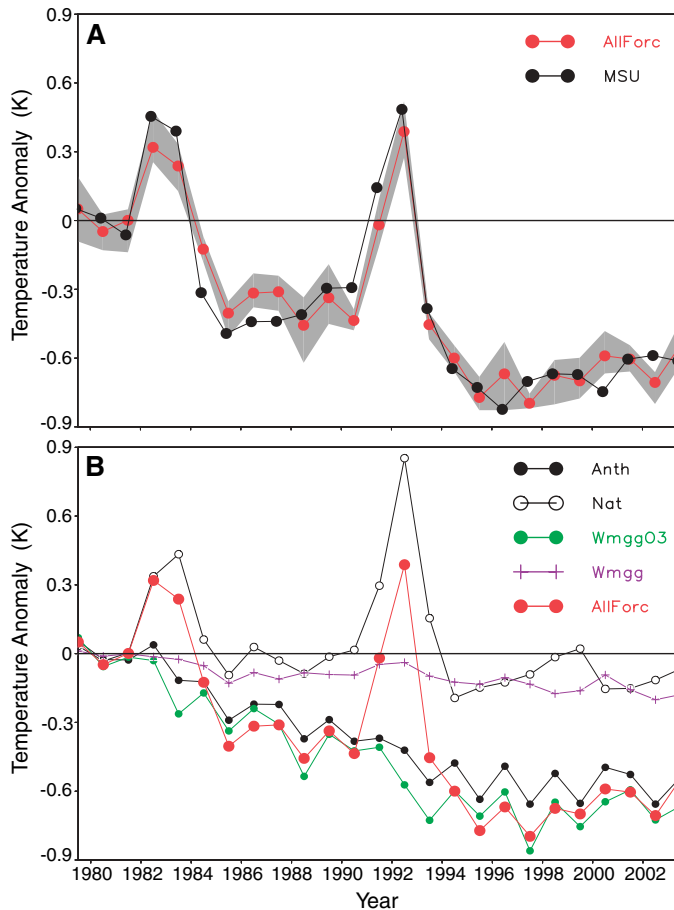
B and C) exhibit a progressive greenhouse gas–dominated cooling of the global stratosphere (*4*–*10*, *22*), with more cooling in the 1990s than in the 1980s. Anth generally has less cooling than WmggO3 at low latitudes. This difference is essentially due to solar warming by anthropogenic upper tropospheric aerosols in Anth (*18*, *23*), with the effect implicitly sampled by the T4 weighting function (*3*–*5*). The increased cooling in AllForc (Fig. 1B) during ~1994–2000 arises primarily from Anth (Fig. 2C), together with a smaller contribution from Nat (Fig. 2A). In contrast, during ~1985–1990, Nat in some domains slightly offsets the Anth cooling (Fig. 2, A and C). Clearly, both Anth and Nat are needed to explain the AllForc evolution and to account for the observed space-time T4 pattern (Fig. 1A).

Figure 3A illustrates that the AllForc simulation successfully captures the complex observed time evolution of the global and annual mean T4 anomalies. The amplitudes of the observed and simulated cooling are very similar, both for the first "step" (1985–1990 minus 1979–1981; results are –0.40 and –0.38 K, respectively) and the second "step" (1994–2000 minus 1985–1990; results are –0.32 and –0.29 K, respectively). The model also replicates the relatively steady behavior of the observed T4 anomalies over ~1994–2000 and the slight temperature increase between the late 1990s and 2003. These results enhance our confidence in the reliability of the

model and the applied forcings. Externally forced changes in AllForc are large relative to the model's internally generated variability (Fig. 3A).

In Fig. 3B, the comparison of WmggO3 and Wmgg shows that the overall lower stratospheric temperature decline is driven primarily by the depletion of ozone, and to a lesser extent by the increase in well-mixed greenhouse gases. Although the T4 Anth anomaly is less than WmggO3 because of the previously mentioned solar heating by anthropogenic aerosols in the upper troposphere (see also Fig. 2, B and C), both exhibit a gradual increase of cooling until the mid- to late 1990s. In contrast, the global average Nat lacks an overall global mean cooling trend but contributes to the AllForc cooling in both decades and is comparable to Wmgg in specific nonvolcanic years.

In the first steplike cooling transition in ~1985, the changes in well-mixed gases and ozone produce an increase in the cooling anomaly of Anth relative to the pre-eruption value (Figs. 2, B and C, and 3B). In contrast to Nat, there is a distinctly increasing cooling of Anth over 1985–1990 (Fig. 3B). During the ~2-year presence of volcanic aerosols, the surface-troposphere system cools; after the aerosols decay, the surface and troposphere temperatures recover, but do so slowly owing to the thermal inertia of the oceans (*9*, *10*, *24*). The cooler surface and troposphere reduce the upwelling long-

wave radiation flux, resulting initially in a slight cooling anomaly of the lower stratosphere in Nat. Added to this is the effect of solar cycle variations, yielding decreases in irradiance during the mid-1980s (*1*, *14*). The net result is an approximately steady AllForc anomaly over ~1985–1990 (Figs. 1B and 3B).

The second steplike cooling transition in ~1994 is followed by another near-steady anomaly period (~1994–2000; Fig. 3B). The sharp decline in Anth relative to the pre-eruption value is due to WmggO3 (Figs. 2, B and C, and 3B). In contrast to 1985–1990, stratospheric ozone depletion in the 1990s is easily the principal contributor to the Anth and AllForc cooling. This depletion levels off during the mid- to late 1990s, resulting in a near-flattening of the WmggO3 and Anth anomalies. After ~1998, the cooling anomaly in WmggO3 decreases slightly, consistent with a lesser ozone depletion. The Nat cooling contribution again comprises a post–volcanic-aerosol cooling of the surface and troposphere as in the mid-1980s, plus the effect of another minimum in the solar cycle (*14*). In the mid-1990s, the Nat cooling (Fig. 2A), together with Anth (Fig. 2C), yields a substantial AllForc cooling (Figs. 1B and 3B). By the mid- to late 1990s, the Nat cooling contribution diminishes as the surface-troposphere system recovers from the volcanic cooling and the solar cycle proceeds to its next maximum (*14*). Thus, the deceleration of the AllForc cooling in the mid- to late 1990s (Figs. 1B and 3B) is traceable to stratospheric ozone changes coupled with natural influences.

The two steplike temperature transitions, followed by relatively steady periods (Figs. 1 and 3A), are thus a consequence of both anthropogenic and natural factors. The anthropogenic cooling influence becomes an important global feature by the late 1980s and a dominant one in the 1990s (Figs. 2, B and C, and 3B). Although the effect of volcanic aerosols on the transient warming in the lower stratosphere is known (*4*, *5*, *9*, *10*), the results here show that natural forcing, despite lacking a trend, has contributed to the modulation of the 1979–2003 global cooling evolution. If the solar and volcanic aerosol forcing were entirely absent, the temperature evolution would have comprised a steady decrease driven by Anth, but this is inconsistent with the observations (Figs. 1A and 3B). The decadal-scale temperature decline that is dominated by stratospheric ozone depletion is very likely unprecedented in the historical evolution of the lower stratospheric thermal state. The juxtaposition of the 1979–2003 ozone loss, solar variation, and volcano effects in yielding the observed temperature evolution is also likely to be unusual.

In the 21st century, if ozone depletion were to continue unabated, the anthropogenic effects would outweigh natural forcing to an even greater extent than in the 1990s (Fig. 3B). The comparable value of the Nat cooling anomaly to that of Wmgg in years without volcanic

aerosol influences (Fig. 3B) presents another implication for the future. With stratospheric ozone anticipated to recover over the next several decades because of a reduction in halogen loadings, and before the continued increase in well-mixed greenhouse gases enables them to be the dominant factor, natural forcing contributions to the global lower stratospheric temperature evolution could become relatively more important than in the period considered here.

An uncertainty in these quantitative estimates is the incomplete knowledge of the global vertical profile of ozone change immediately after volcanic eruptions (25, 26). Enhancements in global ozone loss due to volcanic aerosols, as indicated by chemical modeling (27) and not incorporated in the data set used here, could add to the simulated cooling. Including explicit stratospheric chemistry (28, 29) in future coupled atmosphere-ocean climate model simulations would provide further insights into the evolution of cooling. An increase in lower stratospheric water vapor will also contribute to a cooling (8, 30), although its space-time evolution is uncertain (31). Another uncertainty is the extent to which upper tropospheric species (such as aerosols) affect T4 temperatures. The observed variations in stratospheric ozone likely contain influences due to dynamical fluctuations, such as changes in planetary waves and stratosphere-troposphere coupling (1) and the perturbation of tropical stratospheric circulation due to volcanic aerosol heating (32). This suggests that internal system variations in ozone will affect global temperature changes, but probably much less than the large anthropogenic ozone loss over the period. Despite the uncertainties, the simulations described here quantitatively demonstrate the existence of an externally forced response in the observed 1979–2003 global lower stratospheric temperature time series, and they delineate the natural and anthropogenic influences on the evolution of the cooling.

References and Notes

1. M. P. Chipperfield et al., in Scientific Assessment of Ozone Depletion: 2002 (report no. 47, Global Ozone Research and Monitoring Project, World Meteorological Organization, Geneva, Switzerland, 2003), chap. 4.
2. D. Thompson, S. Solomon, J. Clim. 18, 4785 (2005).
3. D. Seidel, J. Lanzante, J. Geophys. Res. 109, 10.1029/2003JD004414 (2004).
4. V. Ramaswamy et al., Rev. Geophys. 39, 71 (2001).
5. B. D. Santer et al., Science 309, 1551 (2005).
6. U. Langematz, M. Kunze, K. Krueger, K. Labitzke, G. L. Roff, J. Geophys. Res. 108, 10.1029/2002JD002069 (2002).
7. V. Ramaswamy, M. D. Schwarzkopf, Geophys. Res. Lett. 29, 10.1029/2002GL015141 (2002).
8. K. P. Shine et al., Quart. J. R. Soc. Meteorol. 129, 1565 (2003).
9. B. D. Santer et al., Science 301, 479 (2003).
10. J. E. Hansen et al., J. Geophys. Res. 107, 10.1029/2001JD001143 (2002).
11. The Geophysical Fluid Dynamics Laboratory coupled atmosphere-ocean model CM2.1 (12) is used to investigate the responses to natural and anthropogenic forcings. The atmospheric component of the model has 2°-by-2.5° latitude-longitude resolution and 24 vertical levels, with 5 in the stratosphere; the top is at 40 km. The horizontal resolution of the ocean component of the model is 1°, with the latitudinal spacing reducing to $\frac{1}{3}$° near the equator; there are 50 vertical levels.
12. T. Delworth et al., J. Clim., in press.
13. T. R. Knutson et al., J. Clim., in press.
14. J. Lean, G. Rottman, J. Harder, G. Kopp, Solar Phys. 203, 27 (2005).
15. G. Stenchikov et al., J. Geophys. Res., in press.
16. The observed temporal evolution of the well-mixed greenhouse gases (carbon dioxide, methane, nitrous oxide, and halocarbons) is employed in the model [(13) see the supporting online material (SOM)] in a manner similar to that of (33).
17. Zonally and monthly averaged concentrations of stratospheric ozone are based directly on observations involving a combination of satellite and polar ozonesonde measurements [(25, 26) see SOM]. A standard regression analysis of the data over the period is performed, comprising terms that represent solar variations and QBO influences, along with a function representing the stratospheric ozone loss trend based on the time series of the equivalent effective stratospheric chlorine (26). In view of the dominant influence of the halogen-induced depletion in the lower stratosphere over the period, stratospheric ozone change is taken to be part of the anthropogenic forcing.
18. Spatial distribution and temporal variations of tropospheric short-lived species (ozone and aerosols) are simulated by a global chemistry-transport model [(34, 35) see SOM]. The vertical profiles of tropospheric and stratospheric ozone distributions are smoothly merged at the tropopause. Tropospheric aerosol species consist of dust, sea salt, black and organic carbon, and sulfate, with the respective optical properties taken from (36); dust and sea salt are presumed to be unaffected by anthropogenic activity.
19. C. Mears, M. Schabel, F. Wentz, J. Clim. 16, 3650 (2003).
20. W. J. Randel, F. Wu, R. Swinbank, J. Nash, A. O'Neill, J. Atmos. Sci. 56, 457 (1999).
21. K. Labitzke, H. van Loon, J. Meteorol. Soc. Jpn. 73, 883 (1995).
22. Although the increase in tropospheric ozone over the period reduces the radiative flux convergence and thus also yields a general cooling in the lower stratosphere, its contribution is substantially less than that due to stratospheric ozone loss (37).
23. P. Ginoux et al., in preparation.
24. A. J. Broccoli et al., J. Geophys. Res. 108, 10.1029/2003JD003812 (2003).
25. W. J. Randel, F. Wu, Geophys. Res. Lett. 26, 3089 (1999).
26. W. J. Randel et al., in preparation.
27. S. Solomon et al., J. Geophys. Res. 101, 6713 (1996).
28. M. Dameris et al., Atmos. Chem. Phys 5, 2121 (2005).
29. J. Austin, R. J. Wilson, in preparation.
30. P. Forster, K. P. Shine, Geophys. Res. Lett. 26, 3309 (1999).
31. W. J. Randel, F. Wu, S. J. Oltmans, K. Rosenlof, G. E. Nedoluha, J. Atmos. Sci. 61, 2133 (2004).
32. G. Stenchikov et al., J. Geophys. Res. 107, 10.1029/2002JD002090 (2002).
33. V. Ramaswamy et al., in Climate Change 2001: The Scientific Basis. Contribution of Working Group I to the Third Assessment Report of the Intergovernmental Panel on Climate Change, J. T. Houghton et al., Eds. (Cambridge Univ. Press, Cambridge, 2001), pp. 349–416.
34. L. W. Horowitz et al., J. Geophys. Res. 108, 10.1029/2002JD002853 (2003).
35. X. Tie et al., J. Geophys. Res. 110, 10.1029/2004JD005359 (2005).
36. J. M. Haywood, V. Ramaswamy, B. J. Soden, Science 283, 1299 (1999).
37. V. Ramaswamy, M. Bowen, J. Geophys. Res. 99, 18909 (1994).
38. The authors acknowledge J. Lean for the solar irradiance data set (including updates) and assistance in understanding the solar forcing. E. Dlugokencky is acknowledged for the update in the estimates of the observed well-mixed greenhouse gas concentrations. Comments by two reviewers are greatly appreciated.

Molecular Linkage Between the Kinase ATM and NF-κB Signaling in Response to Genotoxic Stimuli

Zhao-Hui Wu, Yuling Shi, Randal S. Tibbetts, Shigeki Miyamoto*

The transcription factor NF-κB modulates apoptotic responses induced by genotoxic stress. We show that NF-κB essential modulator (NEMO), the regulatory subunit of IκB kinase (IKK) (which phosphorylates the NF-κB inhibitor IκB), associates with activated ataxia telangiectasia mutated (ATM) after the induction of DNA double-strand breaks. ATM phosphorylates serine-85 of NEMO to promote its ubiquitin-dependent nuclear export. ATM is also exported in a NEMO-dependent manner to the cytoplasm, where it associates with and causes the activation of IKK in a manner dependent on another IKK regulator, a protein rich in glutamate, leucine, lysine, and serine (ELKS). Thus, regulated nuclear shuttling of NEMO links two signaling kinases, ATM and IKK, to activate NF-κB by genotoxic signals.

The NF-κB family of transcription factors is an important point of convergence for many signal transduction pathways, which regulate genes that are critical for processes such as development, innate and adaptive immune responses, cell migration, and apoptosis (1). NF-κB regulates apoptosis and is an attractive target for anticancer drug development (2). Inactive NF-κB is cytoplasmically localized because of its association with inhibitor proteins, such as IκBα. Distinct signaling

Department of Pharmacology, University of Wisconsin–Madison, 301 SMI, 1300 University Avenue, Madison, WI 53706, USA.

*To whom correspondence should be addressed. E-mail: smiyamot@wisc.edu